Apodization Functions in Fourier Transform Ion Mobility Spectrometry

Robert H. St. Louis,*[1] William F. Siems, and Herbert H. Hill, Jr.

Chemistry Department, Washington State University, Pullman, Washington 99163

Ion mobility spectrometry is a sensitive and selective detection method following capillary chromatography. Fourier transform ion mobility spectrometry (FT-IMS) is capable of collecting a complete mobility spectrum of a high-resolution chromatographic peak during its few seconds of residence in the spectrometer. An apodization function is a mathematical transformation carried out on data received from an interferometer to alter the instrument's response function before the Fourier transformation is calculated to obtain the spectrum. Peak broadening and base-line instabilities reported in earlier Fourier transform ion mobility studies can be eliminated using apodization functions. In this work, the resolution and sensitivity effects of various apodization functions applied to IMS interferograms are demonstrated. The studied functions include Hann, Hamm, super-Gaussian, and rectangular. Also, in this paper, spectral response, resolution, and noise were monitored as the FT-IMS frequency scan range was varied from 2.0 to 20.0 kHz. Comparisons are made between the frequency scan range in Fourier transform IMS and the pulse width in signal-averaged IMS. FT-IMS was shown to have signal/noise improvements of >3× over signal-averaged IMS under conditions of high resolution.

INTRODUCTION

Ion mobility spectrometry (IMS) is an atmospheric pressure, electrophoretic analytical technique that separates ions on the basis of their gas-phase mobilities (*1*, *2*). Analytical interest in the technique is derived from its excellent detection limits, speed of response, and applicability to numerous organic functionalities (*3–5*). It has developed into an efficient detector following capillary gas (*6–11*) and supercritical fluid chromatography (*12*, *13*).

Ion mobility spectra are traditionally collected with a signal-averaging methodology. The entrance gate is pulsed open for a short duration, typically 0.2 ms or less, and the ions are monitored as a function of drift time for approximately 20 ms. A succession of scans is stored and averaged to produce a single ion mobility spectrum. with this method, only ~1% of the available ions contribute to the mobility signal, thus limiting sensitivity. A larger entrance gate pulse increases the ion signal but at the expense of spectral resolution. In order to make better use of the available ion current, a Fourier transform (FT) mode of operation was developed (*14*). In Fourier transform spectral collection, the entrance and exit gates are controlled by a binary (on, off) scanning square-wave generator. The gates are driven simultaneously by the identical square wave with zero phase delay. The scanning parameter is the square-wave frequency. The entrance gate creates a continuous stream of ion pulses, which drift down the tube with their characteristic drift time, t_d. As the square-wave frequency is varied, ions of different drift time pass in and out of phase with the exit gate generating a mobility interferogram. Fourier transformation of the frequency dispersive interferogram produces the familiar time dispersive ion mobility spectra. With this method, both the entrance and exit gates are open 50% of the time, so up to 25% of the available ions are sampled.

The signal detected, $S(\nu)$, in mobility interferometry is a function of a compound's drift time spectrum and a gate correlation function which determines the fraction of ions transmitted to the collector (*14*).

$$S(\nu) = m(t)e(t,\nu)\ dt$$

$e(t,\nu)$ represents the gate correlation function, which determines the fraction of ions with drift time, t, reaching the collector at frequency ν. $m(t)$ is a compound's drift time spectrum. Figure 1 illustrates a square wave simultaneously applied to the entrance and exit gates and the resultant gate correlation function. The maximum value of $e(t,\nu)$ is $0.5I_o$, where I_o represents the total current with both gates open and 0.5 is the fraction of time the entrance gate is open. The correlation function represents the filtering action of the gates. With a gate modulation frequency ν, the only ions that reach the collector with full intensity have transit times $0, 1/\nu, 2/\nu$ .... The only ions which do not reach the collector at all have transit times $1/2\nu, 3/2\nu, 5/2\nu$ .... If $m(t)$ consists of a single ion of drift time t, then $S(\nu)$ is also a triangle wave with maxima and minima:

$$S(\nu)_{max} = 0.5I_o \qquad \nu = 0, 1/t, 2/t, 3/t, ...$$

$$S(\nu)_{min} = 0 \qquad \nu = 1/2t, 3/2t, 5/2t, ...$$

If $m(t)$ consists of a number of ions of different drift times, then $S(\nu)$ will be the sum of interfering triangle waves.

Since the interferogram is obtained using a finite frequency range (ν_1, ν_2), the interferogram as measured is truncated by multiplication with an apodization function.

$$S(\nu') = S(\nu) \times \text{apodization}$$

In previously published literature (*14–16*), this apodization function has been a rectangular window, $f(\nu_1,\nu_2)$. Where $f(\nu_1,\nu_2)$ has a value of 1 in the range (ν_1, ν_2) and 0 outside of it. Fourier transformation of $S(\nu')$ when a rectangular window function was used produced time dispersive ion mobility spectra with broadened ion peaks and increased base-line noise, relative to signal-averaged IMS. An example is seen in Figure 2. The objective of this work was to apply other apodization functions to mobility interferometry and to quantify its effects on spectral resolution and signal/noise. The functions to be studied include Hann, Hamm, and super-Gaussian.

Previously published experiments (*14–17*) utilizing Fourier transform ion mobility spectrometry (FT-IMS) have used relatively narrow frequency ranges (5000–10 000 Hz). In this study, frequency scan ranges up to 20 000 Hz were investigated. Spectral resolution and signal intensity were monitored as the frequency scan range was varied from 2000 to 20 000 Hz. Instrumental resolution in FT-IMS is controlled by the frequency scan range and is inversely related to the pulse width in signal-averaged IMS. A secondary objective of this work was to compare the signal/noise ratios of Fourier

[1] Current address: Physical and Analytical Research, Building 150A, Eastman Chemical Co., Kingsport, TN, 37663.

0003-2700/92/0364-0171$03.00/0

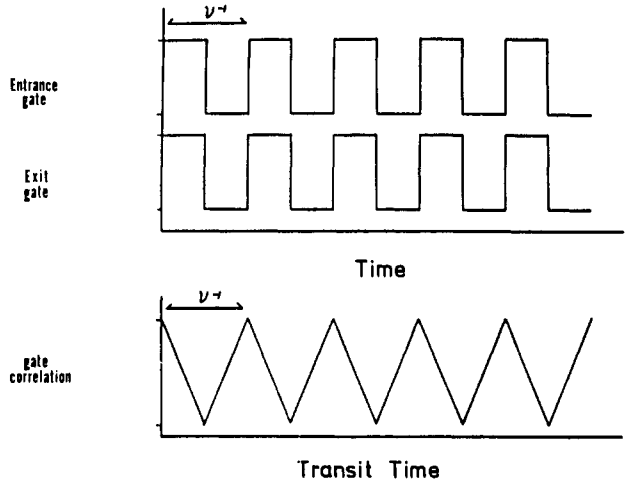

Figure 1. Gate correlation function with a square wave simultaneously applied to the entrance and exit gates.

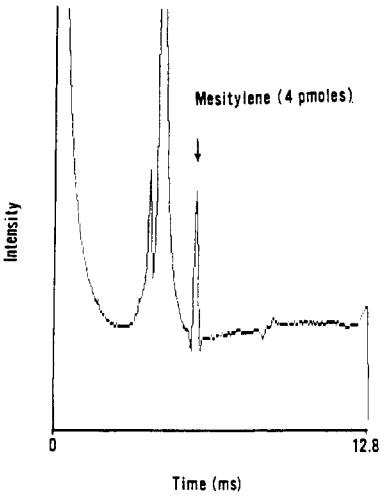

Figure 2. Ion mobility spectrum, 4 pmol of mestitylene. Frequency-dispersive interferogram was Fourier transformed after multiplication by a rectangular window function.

transform and signal-averaged IMS under conditions of high resolution.

EXPERIMENTAL SECTION

Instrumentation. The ion mobility spectrometer used in this work has been described in detail previously (*9*). It was designed principally as a detector following capillary gas chromatography. A schematic diagram of the system when being operated in the Fourier transform mode is shown in Figure 3. Samples were introduced into a 0.8-cm^3 ionization source lined with a ^{63}Ni foil (E. I. du Pont de Nemours, Billerica, MA) of total activity 15 mCi of β radiation through a capillary column from a Hewlett-Packard 5890 GC system. The column was 5% phenyl 95% methyl silicone (DB-5, J&W Scientific, Folsom, CA), 22 m, 0.25-mm i.d., 0.25-μm film thickness.

Gate signals were controlled by a scanning square-wave generator (SSQ) custom designed by Washington State University Technical Services. Schematic diagrams for the square-wave generator have been published previously (*17*). The SSQ can perform square-wave scans in the range of 20–20 020 Hz with scan times down to 0.1 s. Synchronization of data collection with the square-wave scan is provided by a 250-μs trigger pulse sent to an IBM-XT personal computer. The computer was equipped with a PCI-2000 intelligent instrumentation system (Burr-Brown Corp., Tucson, AZ). The PCI-2000 was designed to turn a personal computer into a system for data acquisition, test, measurement, and control. It included a carrier board, timer module, and analog/digital module.

The electric field was created and maintained by a high voltage applied directly to the ionizer from a ±5000-V power supply

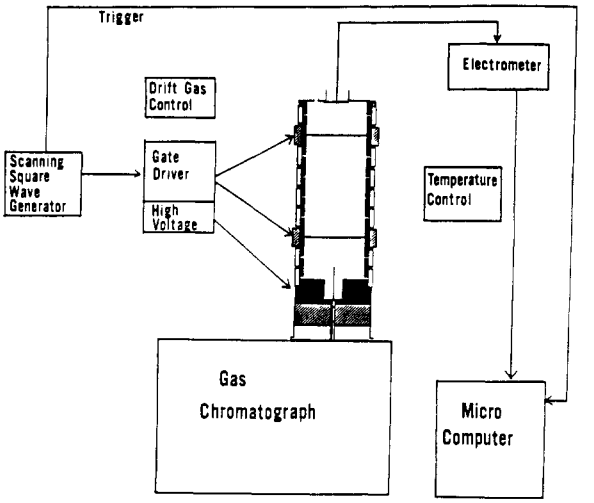

Figure 3. General schematic of a Fourier transform ion mobility spectrometry system. Gate signals are controlled by a scanning square-wave generator. Spectral collection is synchronized with the square-wave scan by a trigger pulse sent to a IBM-XT personal computer.

(Bertan Assoc., Syosset, NY). This voltage was dropped to ground via a series of 1-MΩ resistors connected to successive guard rings. The signal was amplified by a Keithley Model 427 electrometer (Keithley Instruments, Cleveland, OH) and sent to the IBM-XT personal computer for signal processing.

Preheated drift gas entered through an inlet in the top of the spectrometer. The drift gas flow rate was controlled by an Airco 752 rotameter. Temperature to the spectrometer was maintained with a Digisense Model 2168-70 temperature controller (Cole Parmer, Chicago, IL). Experiments were designed to measure the effects on Fourier transform spectral resolution, signal, noise, and signal/noise of varying the frequency scan range of the system. For comparison, experiments were performed in both Fourier transform and signal-averaging modes of operation. The aperture grid was removed when operating in the Fourier transform mode.

Frequency Scan Range. Instrumental resolving power in FT-IMS is controlled by the frequency scan range applied to the gates by the scanning square-wave generator. For example, a frequency range of 20–20 000 Hz has greater resolving power than a range of 20–5000 Hz. Instrumental resolution in signal-averaging IMS is controlled by the pulse width applied to the entrance gate. Equivalent instrumental resolution for the two methods can be obtained by utilizing the following relationship:

$$\text{frequency range (kHz)} = 1/\text{pulse width (ms)}$$

Equivalent pulse widths and frequency scan ranges are presented below.

pulse width, ms	frequency range, kHz
0.50	2.0
0.20	5.0
0.10	10.0
0.067	15.0
0.050	20.0

In our initial experiment, resolving power and signal intensity were monitored for the major reactant ion peak as the above instrumental values for the frequency scan range (in FT-IMS) and pulse width (in signal-averaging IMS) were used.

Resolving power was measured in a manner analogous to capillary electrophoresis or chromatography as the number of plates. Plate number was defined by

$$n = (t_d/\sigma)^2 = 5.54(t_d/W_h)^2$$

where n equals the plate number, t_d equals the drift time of the ion, σ equals the standard deviation of the ion peak, and W_h equals the peak width at half-height.

FT conditions were as follows: high voltage, 2700 V (308 V/cm); gate voltage, ±30 V; rise time, 10 ms; drift gas flow rate, 300

Table I. Apodization Values as a Function of the Data Point in the Digitized Interferogram

data point	Hann	Hamm	super-Gaussian[a]
1	0.00004	0.0800	0.00001
50	0.0916	0.1642	0.1962
100	0.3327	0.3861	0.8752
150	0.6351	0.6643	0.9959
200	0.8880	0.8970	0.9999
250	0.9989	0.9989	1.0000
300	0.9230	0.9328	0.9999
350	0.6988	0.7229	0.9986
400	0.3977	0.4459	0.9372
450	0.1342	0.2034	0.3872
500	0.0046	0.0842	0.0006
510	0.00004	0.0800	0.00002

[a] For super-Gaussian window, $\epsilon = 0.000\,01$ and $P = 9$.

mL/min N_2; temperature, 225 °C; apodization function, Hann window; scan time, 8.1920 s.

Signal-averaging conditions were identical to FT conditions except as follows: The rise time for pulse widths 0.1, 0.2, and 0.5 ms was 0.1 ms. For pulse width 0.05 ms, the rise time was 0.01 ms. For pulse width 0.067 ms, the rise time was 0.03 ms. The reason for this variation is discussed under Results and Discussion. The scan time was 25.60 ms with 256 scans averaged for a total time 6.5536 s.

Apodization Functions. The Fourier transform algorithm in the MicroWay Fast Fourier Transform software package was applied to the mobility interferogram as though the end points of the wave form were joined to each other around a circular axis. The circular sine and cosine functions applied to the circular interferogram then determined the various frequency components. The joining of the mobility interferogram's end points puts a region of strong oscillation (the beginning) next to a region of weak oscillation (the end) and introduces a square-edged step into the interferogram. This can be visualized by looking at Figure 4a and imagining the end of the interferogram (frequency, 5 kHz) wound around and connected to the beginning (frequency, 20 Hz), forming a cylindrical ring. It is this square-edged step where the end of the interferogram meets the beginning that produces the spectral peak broadening and base-line instabilities that are noted when a rectangular window function is used. The function of the Hann, Hamm, or super-Gaussian window is to replace this square-edged step with a gradual curve more amenable to transformation.

The Hann window is mathematically

$$\mathrm{HNW}(n) = \tfrac{1}{2}(1 - \cos\,[2\pi n/(N-1)])$$

where n is the data point in the digitized interferogram and N is the number of points in the interferogram: $n = 0, 1, 2, \ldots (N-1)$, where $N = 2^m$, with m equal to an integer ($m = 9$ throughout this work). The Hann window, with maximum values near the center of the interferogram tapers to zero as n approaches 0 or $(N-1)$, the beginning and end of the interferogram. The value of the apodization functions at increasing data points is shown in Table I. Figure 4b shows the resultant mobility interferogram after multiplication of the raw data of Figure 4a by the Hann window. If Figure 4b were wound into a cylindrical ring, there would be no discontinuities: a gradual increase and decrease in interferogram intensity would be presented to the FT algorithm.

The mathematical expression for the Hamm window is

$$\mathrm{HMW}(n) = 0.54 - 0.46\,\cos\,[2\pi n/(N-1)]$$

The Hamm window resembles the Hann window in many respects, but as n approaches zero or $(N-1)$, it tapers the signal to 0.08. Figure 4c shows the resultant mobility interferogram after multiplication of the raw data of Figure 4a by the Hamm window.

The super-Gaussian window function is mathematically

$$\mathrm{SGW}(n) = e^{-|(2n-N)/A|^P}$$

where $A = N(-\ln \epsilon)^{-1/P}$, P = power, $2 < P < 128$, and ϵ = ratio, $\epsilon < 1$. In this expression, n is the data point number in the digitized interferogram and N is the number of points in the interferogram. The power, P, and the ratio, ϵ, are values which can be input by the user as befits their needs. Figure 4d shows the resultant mobility interferogram after multiplication of the raw data of Figure 4a by the super-Gaussian window with a power of 9, and a ratio of 0.000 01. The ϵ term controls the value of the window as n goes to zero. The lower the value of ϵ, the closer the value of the window approaches zero as n approaches zero. The P term controls the slope at which the window reaches maximum intensity. A larger value of P corresponds to a steeper slope.

The purpose of this work was to determine the effect of these windowing functions on Fourier transform spectral resolving power

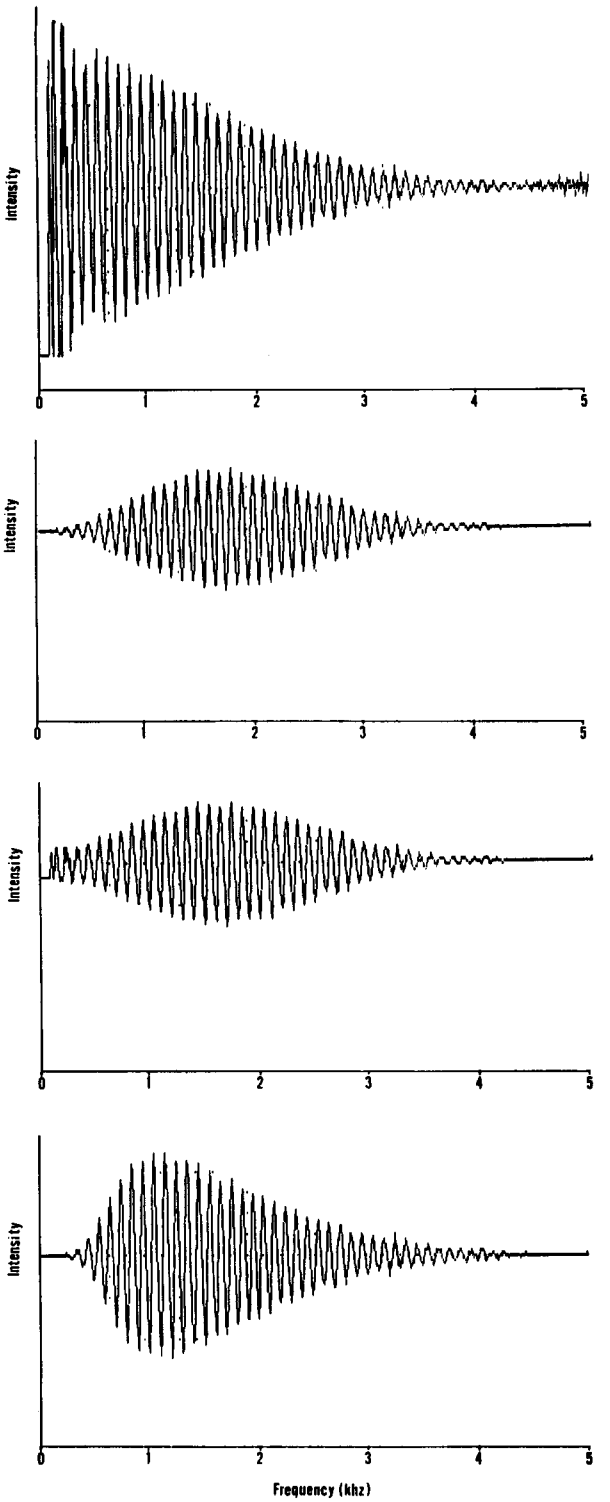

Figure 4. Frequency-dispersive interferogram multiplied by (from top to bottom) (a) a rectangular window function, (b) a Hann window function, (c) a Hamm window function, or (d) a super-Gaussian window function ($\epsilon = 0.000\,01$, $p = 9$).

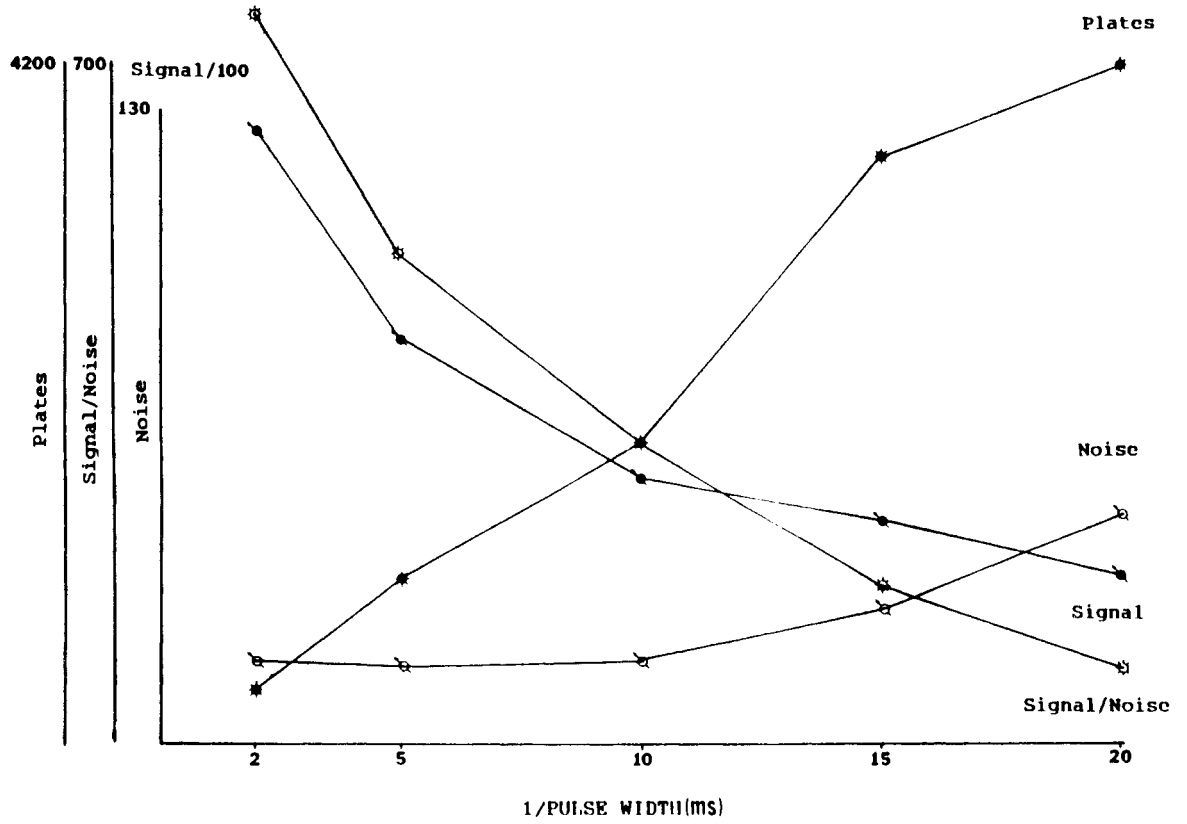

Figure 5. Spectral response vs 1/pulse width in signal-averaged IMS.

and signal intensity. Mobility data were collected for the background reactant ions and for 4 pmol of mesitylene introduced into the ion mobility spectrometer by capillary gas chromatography. This data set was then truncated by either the rectangular, Hann, Hamm, or super-Gaussian windows. The values of ϵ and P in the super-Gaussian window were also varied and the resultant changes in spectral resolution and sensitivity monitored. Spectrometer conditions were as follows: voltage, 2200 V (E = 250 V/cm); temperature, 225 °C; drift gas flow rate, 1400 mL/min N_2; scan time, 8.1920 s; sampling frequency, 62.5 Hz; data points, 512; frequency scan range, 20–20 020 Hz. Chromatographic conditions were as follows: injector temperature, 225 °C; oven temperature, 90 °C; carrier gas flow rate, 0.9 mL/min He.

RESULTS AND DISCUSSION

Frequency Scan Range. In signal-averaging IMS, the maximum resolving power of the system can never be less than the initial pulse, t_0, of ions introduced into the drift space of the spectrometer. Thus, there is a desire for narrow entrance gate pulses in order to maximize the separation power of the system. Signal intensity, however, is improved by using a wide entrance gate pulse. The wider the initial pulse is, the greater the amount of available current will be. These results can be seen in Figure 5, a multiple y scale plot monitoring changes in plates, signal intensity, noise, and signal/noise as a function of 1/pulse width. The inverse relationshp between resolving power (as measured by plates) and signal intensity is directly apparent. In signal-averaging IMS, this has often led to compromised conditions of moderate resolution and moderate sensitivity. For example, pulse widths of 0.10 or 0.20 ms (1/pulse width = 10 or 5) have often been used.

Also demonstrated in Figure 5 is increased noise with narrow entrance gate pulses. This is attributable to a change in the electrometer rise time. For pulse widths of 0.05 ms (1/pulse width = 20) a rise time of 0.01 ms was used, for pulse widths of 0.067 ms (1/pulse width = 15) a rise time of 0.03 ms was used. For all other pulse widths, a rise time of 0.10 ms was used. This decreased rise time was required to accurately monitor current changes with narrow pulses. If 0.10-ms rise times were used with the 0.05- and 0.067-ms pulse widths, decreased plate values were obtained.

pulse width, ms	rise time, ms	plates
0.05	0.1	2740
0.05	0.01	4159
0.067	0.1	2283
0.067	0.03	3574

Increased noise is thus an undesirable side effect of maximizing the resolving power of signal-averaged IMS. This was reflected in the rapid negative slope of signal/noise in Figure 5.

In Fourier transform IMS, the instrumental parameter comparable to pulse width is the frequency scan range. The minimum peak width measurable is equal to 1/scan range. For example, a 20-kHz scan range is comparable to a pulse width of 1/20 kHz or 0.05 ms. Figure 6 is the Fourier transform data analogous to the signal-averaged data of Figure 5. An inverse relationship between plates and signal intensity is observed, similar to that in Figure 5. The decreased signal intensity at high-frequency ranges is probably due to two factors, gate depletion (*18*) and the fact that the higher proportion of the signal intensity is located in the low-frequency end of the spectrum. In this experiment, 512 data points were taken over a scan time of 8.1920 s. These values were maintained for all frequency scan ranges. The final data from these experiments were multiplied by a Hann window function. The purpose of this function was to gradually reduce the interferogram data to zero at the beginning and end of the spectrum, the result of which was that much of the high-signal and high-noise data at the low-frequency end of the spectra were removed. This effect was magnified at high-frequency ranges, since a greater portion of the frequency range was displaced to the portion of the data removed by the Hann window. The result was decreased signal and noise at high-frequency ranges.

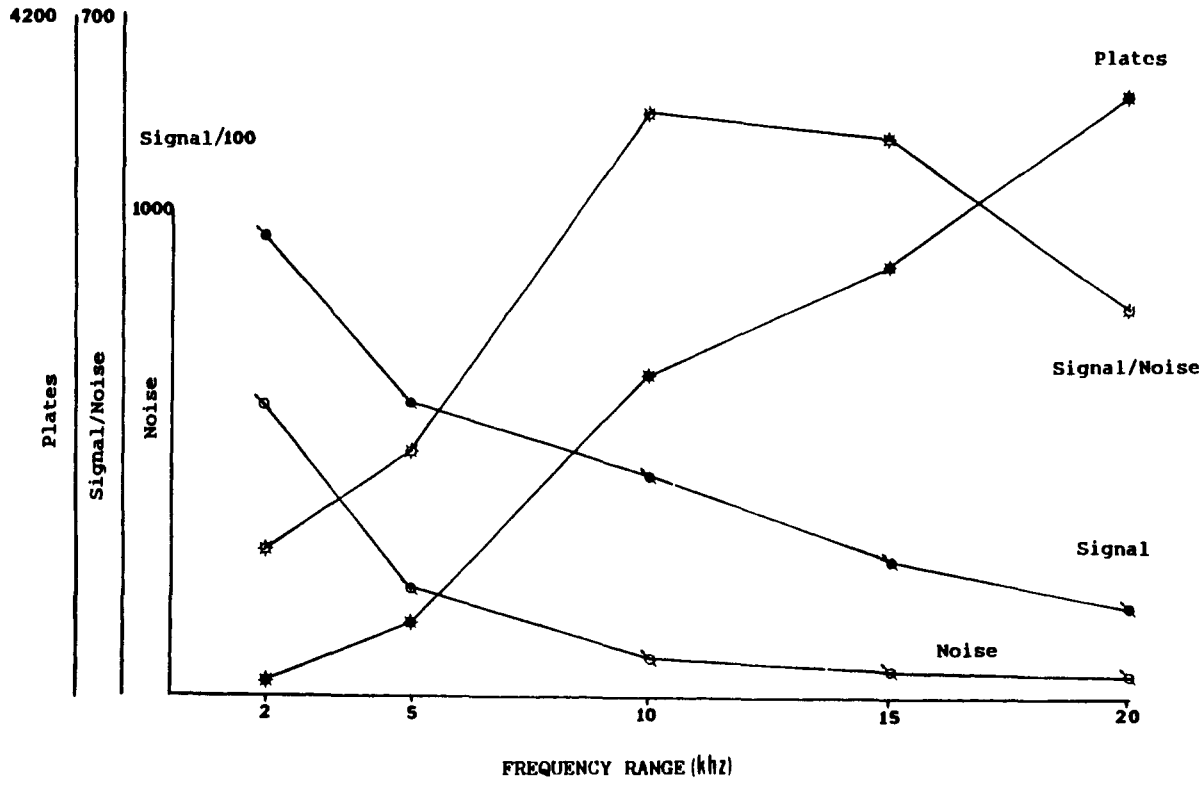

Figure 6. Spectral response vs the frequency scan range in Fourier transform IMS.

Signal intensity can also be decreased at higher pulse frequency by a phenomenon referred to a gate depletion. Gate depletion occurs because, when the gate is closed, the distribution of ions upstream of the gate is altered by the electrostatic field near the gate in such a way that, when the gate is opened, it takes some time for the full density of signal ions to pass the gate. In addition, when the gate is closed, the field in the gate attracts some of the ions that have already passed the gate, causing additional loss of signal power. Theoretical modeling of the gate depletion effect has been reported (*18*), but quantitative comparison of experimental results with theoretical calculations has not been performed.

In Figure 6, it is seen that while signal intensity is reduced at high-frequency scan ranges, so is the noise. Consequently, signal/noise values at maximum resolving conditions are high. At a frequency scan range of 20 kHz, approximately 3800 plates were observed, with a signal/noise of 400 for the dominant reactant ion. From Figure 8, a signal-averaged ion mobility spectrum with 3800 plates for the dominant reactant ion would have a signal/noise value of approximately 140. Thus, under the conditions of this experiment, at maximum resolving power, Fourier transform IMS provided 3× the signal/noise of signal-averaged IMS.

Apodization Functions. A Fourier transform ion mobility interferogram was collected for 4 pmol of mesitylene introduced into the spectrometer by capillary gas chromatography. This interferogram is shown in Figure 7. This frequency-dispersive interferogram was then multiplied by either the rectangular, Hann, Hamm, or super-Gaussian window functions and Fourier transformed to produce time-dispersive ion mobility spectra. The resultant ion mobility spectra are shown in Figure 8. Table II quantifies the spectral changes in signal intensity, root-mean-square noise (N_{rms}), signal/N_{rms}, and chromatographic plates for the mesitylene product ion as a function of the window multiplied by the interferogram.

Signal intensity increases in the order Hann < Hamm < super-Gaussian < rectangular. These values essentially reflect the percentage of the intensity data removed by the window. This can be qualitatively visualized by looking at the interferograms in Figure 4. The greatest amount of intensity information was available with the rectangular window. The lowest amount of signal intensity was observed with the Hann function, which tapers the signal to zero at the end points and only gradually increases the window value with increases in n. The Hamm window provided slightly more intensity information by tapering to 0.08 rather than zero. The super-Gaussian window tapers to zero but then increases with a much more rapid slope (with $P = 9$) to provide the second

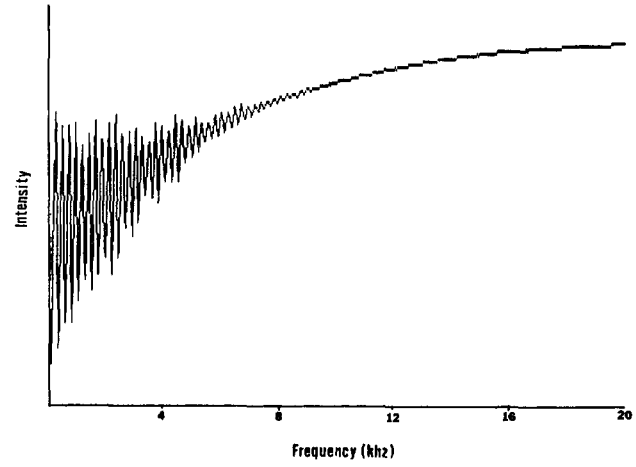

Figure 7. Raw mobility data, 4 pmol of mesitylene.

Table II. Response vs Window Function (Mesitylene Product Ion)

window	signal	N_{rms}	signal/N_{rms}	plates
Hann	23 946	289	82.9	3462
Hamm	31 835	531	60.0	5602
SGW[a]	55 408	664	83.4	2351
rectangular	118 510	3898	30.4	10243

[a] For super-Gaussian window, $\epsilon = 0.000\,01$ and $P = 9$.

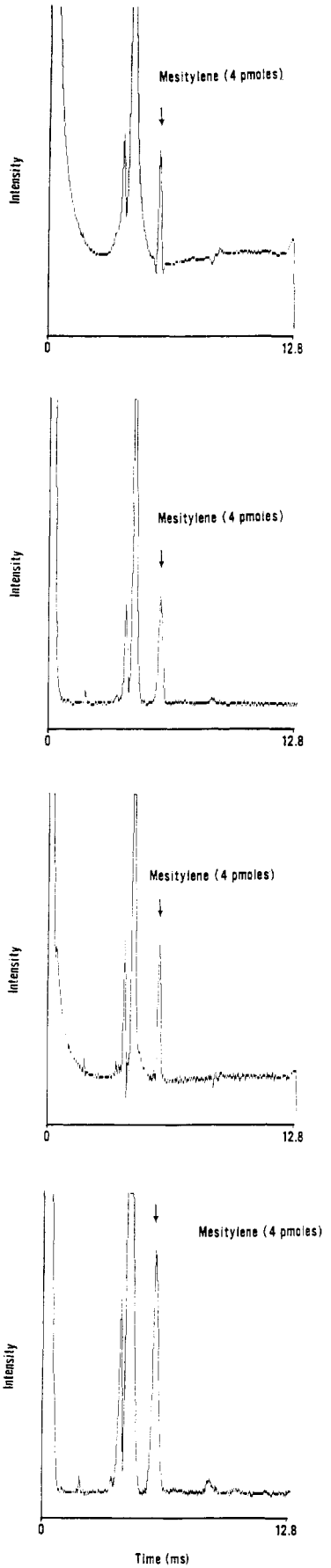

Figure 8. Ion mobility spectrum, 4 pmol of mestiylene. Frequency-dispersive interferogram was Fourier transformed after multiplication by (from top to bottom) (a) a rectangular window function, (b) a Hann window function, (c) a Hamm window function, or (d) a super-Gaussian window function (ϵ = 0.000 01, p = 9).

Table III. Effect of the Ratio and the Power in the Super-Gussian Window (4 pmol of Mesitylene Product Ion)

ϵ	P	signal	N_{rms}	signal/N_{rms}	plates
0.00001	9	55 408	664	83.4	2351
0.0001	9	60 290	698	86.4	2616
0.001	9	66 818	750	89.0	2781
0.01	9	76 400	876	87.2	3126
0.01	5	47 780	570	83.8	3440
0.01	2	14 554	828	51.6	5476
0.03	2	22 309	376	59.3	6671
0.05	2	27 596	449	61.5	7313
0.07	2	31 916	523	61.0	7789
0.10	2	37 415	633	59.1	8254
0.10	5	69 640	960	72.5	5395

highest intensity information.

Noise increased in a similar fashion, indicating the presence of signal-related noise in the interferogram. Noise was also increased, however, by the step function introduced in the Hamm and rectangular window functions when the high-frequency (low-intensity) end of the interferogram was wound around and connected to the low-frequency (high-intensity) end. Signal/N_{rms} was therefore the highest for the Hann and super-Gaussian windows.

The measured plates [plates = $5.54(t_d/W_h)^2$] increased in the order super-Gaussian < Hann < Hamm < rectangular. This indicates the importance of the early portions of the interferogram for resolution as well as intensity information. The data in Table II for the super-Gaussian window were obtained using a ratio (ϵ) of 0.000 01 and a power (P) of 9. Table III quantifies the changes in spectral response as ϵ and P are varied.

The value of ϵ controls the value of the super-Gaussian window as n approaches zero. As the value of ϵ is reduced, the value of the window is lowered. The value of P controls the slope at which the window function reaches maximum intensity. Table III shows that ϵ and P have only minimal effect on signal/N_{rms}, primarily due to the interrelationship between the signal and the noise. Rather large improvements in plates can be obtained, however, at large values of ϵ and small values of P. See, for example, ϵ = 0.10, and P = 2, producing a plate value of 8254.

SUMMARY AND CONCLUSIONS

In this paper, improvements of approximately 3× were obtained for FT-IMS signal/noise values relative to signal-averaged values under conditions of high resolution. Also demonstrated was the importance of the apodization function in FT-IMS, with signal/N_{rms} and spectral resolution varying dependent on the particular function applied to the interferogram. The Hann window probably provides the best compromise between signal/N_{rms} and resolution with the super-Gaussian window providing greater flexibility.

REFERENCES

(1) Cohen, M. J.; Karasek, F. W. *J. Chromatogr. Sci.* **1970**, *8*, 330.
(2) St. Louis, R. H.; Hill, H. H., Jr. *CRC, Crit. Rev. Anal. Chem.* **1990**, *21*, 321.
(3) Carr, T. W., Ed. *Plasma Chromatography*; Plenum Press: New York, 1984.
(4) Hill, H. H., Jr.; Siems, W. F.; St. Louis, R. H.; McMinn, D. G. *Anal. Chem.* **1990**, *62*, 1201A.
(5) Shumate, C.; St. Louis, R. H.; Hill, H. H., Jr. *J. Chromatogr.* **1986**, *373*, 141.
(6) Karasek, F. W.; Hill, H. H., Jr.; Kim, S. H.; Rokushika, S. *J. Chromatogr.* **1977**, *135*, 329.
(7) Baim, M. A.; Hill, H. H., Jr. *Anal. Chem.* **1983**, *55*, 1761.
(8) St. Louis, R. H.; Siems, W. F.; Hill, H. H., Jr. *LC/GC, Mag. Chromatogr. Sci.* **1988**, *9*, 810.
(9) St. Louis, R. H.; Siems, W. F.; Hill, H. H., Jr. *J. Chromatogr.* **1989**, *479*, 221.
(10) St. Louis, R. H.; Siems, W. F.; Hill, H. H., Jr. *J. Microcolumn Sep.* **1990**, *2*, 138.
(11) St. Louis, R. H.; Hill, H. H., Jr. *J. High Resolut. Chromatogr.* **1990**, *13*, 628.

(12) Eatherton, R. L.; Morrissey, M. A., Siems, W. F.; Hill, H. H., Jr. J. High Resolut. Chromatogr. Chromatogr. Commun. 1986, 9, 154.
(13) Hill, H. H., Jr.; Morrissey, M. A. In Modern Supercritical Fluid Chromatography; White, C. M., Ed.; Huthig: Heidelberg, 1988.
(14) Knorr, F. J.; Eatherton, R. L.; Siems, W. F.; Hill, H. H., Jr. Anal. Chem. 1985, 57, 407.
(15) Eatherton, R. L.; Siems, W. F.; Hill, H. H., Jr. J. High Resolut. Chromatogr. Chromatogr. Commun. 1986, 9, 44.
(16) Eatherton, R. L. Ph.D. Thesis, Washington State University, 1987.
(17) Morrissey, M. A. Ph.D. Thesis, Washington State University, 1988.
(18) Aronson, E. A. Sandia Report, Sand 87-0072, UC-32, March 1987.

RECEIVED for Review July 1, 1991. Accepted October 4, 1991.

Elimination of Axial Ejection during Excitation with a Capacitively Coupled Open Trapped-Ion Cell for Fourier Transform Ion Cyclotron Resonance Mass Spectrometry

Steven C. Beu and David A. Laude, Jr.*

Department of Chemistry and Biochemistry, The University of Texas at Austin, Austin, Texas 78712

A Fourier transform ion cyclotron resonance (FT-ICR) mass spectrometer trapped-ion cell is constructed that eliminates the axial ejection of ions during excitation of cyclotron motion. The cell features an open geometry in which the trapping electrodes are extended in the planes of excitation and detection electrodes. A unique aspect of the cell is the capacitive coupling of excitation electrodes to the trap plates to distribute the excitation fields beyond the boundaries of the trapping-potential well. The axial component of the excitation field that is responsible for ejection is eliminated by not terminating excitation electric fields at trap plates that are positioned perpindicular to the magnetic field and thus bound the potential well. Profiles of broad-band mass spectra acquired at increasing excitation energies demonstrate that, even at 0.4-V trap potentials, only mass-independent radial ejection occurs when the excitation is distributed throughout the open cell. In contrast, cells of similar dimension, including both a conventional closed cell at 1.0-V trap potentials and an uncoupled open cell at 0.4-V trap potentials, exhibit severe low-mass ejection during high-power excitation. The open cell is used to acquire laser desorption/ionization mass spectra as evidence of a design simplicity that facilitates immediate integration into more intricate FT-ICR experiments.

INTRODUCTION

Recently, we described a new electrode configuration for the trapped-ion cell of a Fourier transform ion cyclotron resonance spectrometer that was distinguished by the collinear extension of the trapping electrodes in the plane of excitation and detection electrodes (*1*, *2*). This open cell design differed from previous trapped-ion cell designs for FT-ICR that positioned the trap plates perpendicular to the other cell plates (*3–18*). With respect to trapping the ions, the use of open trapping electrodes is similar in concept to previous efforts by physicists to confine electrons and antiprotons for high-precision measurements (*19–24*). Our modeling of open cell trapping and excitation fields suggested a modest reduction in z axis ejection during excitation and a slightly increased shift in the cyclotron frequency associated with the radial trapping field, when compared to the conventional orthorhombic closed cell of similar aspect ratio. These predictions were verified experimentally with an open trapped-ion cell constructed to approximate an elongated orthorhombic cell with an aspect ratio of 2.

Clearly, the original open cell would be recommended, not for improved FT-ICR performance, but rather for important practical considerations in executing the FT-ICR experiment and for increased design flexibility. Examples of practical advantages include increased conductance, the elimination of charging and contamination on trap plates, and both simplified and more efficient introduction of charged particle beams. This latter factor is important for external source applications. The increased flexibility of the open cell derives from the potential to use any combination of collinear electrode segments as trapping, detection, and excitation plates and thereby increases the dimension or number of trapped-ion cells without physical alteration of the electrode assembly. It was also suggested that with appropriate modification of electrical circuitry, these electrodes could simultaneously serve more than one function, with the potential for significant improvement in cell performance (*2*). For example, one suggestion given was that the excitation electrodes could be capacitively coupled to trap plates, thereby creating an axially homogeneous excitation field over the entire length of the trapping-potential well. Not only would the axial component of the excitation field effectively vanish with consequent elimination of z axis ejection during excitation, but with the opportunity to now use very low trap potentials, the deleterious effects of the radial trapping electric field would also diminish.

In previous efforts to minimize z axis ejection, the ions could either be driven to the bottom of the potential well by collisional cooling (*25*) or through an adiabatic ramping of the trapping potential (*26*), or alternatively, the magnitude of the axial excitation fields could be reduced. Examples of this latter approach involve the design of new trapped-ion cells. Caravatti and Allemann distributed the excitation potential over trap plates segmented into 11 electrodes shaped to mimic the radial contour of the electric field (*16*). Wang and Marshall (*17*) and Hanson and co-workers (*18*) reduced both axial excitation and radial trapping fields by distributing the excitation potential over guard wires or rings inserted adjacent to the trap and/or detection electrodes in a manner similar to that employed in the original ICR cell (*27*).

In this manuscript we describe the successful assembly of a capacitively coupled open trapped-ion cell in which the excitation pulse is also applied to the trap electrode segments extending from the two central excitation electrodes. The geometry of this new open cell is identical to the original open cell and therefore retains the practical benefits described above for that cell. Also to be presented is a demonstration of the

0003-2700/92/0364-0177$03.00/0